Saudi Journal of Biological Sciences 25 (2018) 452–456

Contents lists available at ScienceDirect

Saudi Journal of Biological Sciences

journal homepage: www.sciencedirect.com

Original article

Detector location selection based on VIP analysis in near-infrared detection of dural hematoma

Qiuming Sun [a], Yanjun Zhang [a], Jun Ma [a], Feng Tian [a,*], Huiquan Wang [b], Dongyuan Liu [a,b]

[a] Institute of Medical Equipment, Academy of Military Medical Sciences, Tianjin 300161,China
[b] School of Electronics and Information Engineering, Tianjin Polytechnic University, Tianjin 300102, China

ARTICLE INFO

Article history:
Received 26 July 2017
Revised 8 November 2017
Accepted 15 November 2017
Available online 16 November 2017

Keywords:
Detector location screening
Epidural hematoma detection
Variable importance in the projection

ABSTRACT

Detection of dural hematoma based on multi-channel near-infrared differential absorbance has the advantages of rapid and non-invasive detection. The location and number of detectors around the light source are critical for reducing the pathological characteristics of the prediction model on dural hematoma degree. Therefore, rational selection of detector numbers and their distances from the light source is very important. In this paper, a detector position screening method based on Variable Importance in the Projection (VIP) analysis is proposed. A preliminary modeling based on Partial Least Squares method (PLS) for the prediction of dural position μ_a was established using light absorbance information from 30 detectors located 2.0–5.0 cm from the light source with a 0.1 cm interval. The mean relative error (MRE) of the dural position μ_a prediction model was 4.08%. After VIP analysis, the number of detectors was reduced from 30 to 4 and the MRE of the dural position μ_a prediction was reduced from 4.08% to 2.06% after the reduction in detector numbers. The prediction model after VIP detector screening still showed good prediction of the epidural position μ_a. This study provided a new approach and important reference on the selection of detector location in near-infrared dural hematoma detection.

1. Introduction

Dural hematoma often occurs after traumatic brain injury. Inability to make accurate and timely diagnosis for a reasonable treatment plan can result in irreversible brain damage and endanger the life of the patient. Therefore, non-invasive detection of traumatic dural hematoma is always a research focus in the biomedical engineering field (Hitoshi et al., 2016).

Due to the high absorption of 650–900 nm near-infrared light by the hemoglobin molecules within the tissue, the optical properties of the brain tissue tested can be obtained by analyzing the emitting light, so that rapid and non-invasive detection of dural hematoma can be achieved (Wu et al., 2015; Gao et al., 2017). Near-infrared spectroscopy technology has been widely used in clinical applications such as functional neuroimaging (Nourhashemi et al., 2016), brain tumor imaging (Kim et al., 2016; Yildirim et al., 2017), cerebral blood flow measurement (Kato et al., 2015), and brain hematoma detection (Braun et al., 2015). Britton Chance at the University of Pennsylvania in the US has proposed the determination of the presence of cerebral hematoma by comparing the difference between the optical contrast between of two positions in the brain (Robertson et al., 1997). This research further extends this method. Based on the correlation between the differences in near-infrared light density (ΔOD), the degree of hematoma can be analyzed. However, the thicknesses of scalp and skull vary among different individuals due to different growing-up environments, age, race, gender, and other factors. As the thickness of scalp and skull varies, the location of the hematoma changes (Halim and Phang, 2017). Therefore, rational selection of the position and number of detectors is essential for reducing the impact of inter-subject variation and improving the accuracy of the model.

Some researchers have used the tMCimg method to simulate the relationship between the effective depth and the distance between detector and the light source. They concluded that the effective detection depth is twice the distance between the light source and the detector (Wang et al., 2011). Strangman et al. analyzed the effect of the changes in the thickness of scalp and skull on the selection of distances between the light source and the detector. Methods such as the Uninformative Variable Elimination

* Corresponding author.
E-mail address: tianfeng62037@163.com (F. Tian).
Peer review under responsibility of King Saud University.

Production and hosting by Elsevier

https://doi.org/10.1016/j.sjbs.2017.11.044
1319-562X/

(UVE), Synergy Interval Regression and Genetic Algorithm have wide applications in variable selection. The variable importance in the projection (VIP) method examines the importance of independent variables in modeling. This method has been widely applied in fields like epidemiological analysis (Bergdahl and Bergdahl, 2000), remote sensing (Zeng et al., 2010; Shi et al., 2017), biochemical analysis (Broderick et al., 2006), and blood component testing (He et al., 2016). In this study, it is noted that signals detected by the detectors have multiple linear dependencies. Thus, by using the VIP analysis technique, the detectors with strong predictive and interpretative abilities for hematoma can be selected. Through the VIP analysis, the number of detectors was reduced from 30 to 4 in this study and the model's prediction capability was improved (Shamsudin et al., 2017). This study introduced a novel idea for the selection of distance between the near-infrared light source and the detectors, upon which clinical application of hematoma prediction can be applied based on differential near-infrared optical density.

2. Materials and methods

2.1. VIP analysis based on the partial least-squares regression

VIP is an auxiliary analysis technology based on the partial least squares method. It can be used for the determination and selection of important independent variables. When the correlation between variables is strong, it can describe the explanatory power of independent variables to dependent variables through the comprehensive principal components of the relevant independent variables. It also can be used to screen the independent variables based on their VIP abilities and to analyze the explanatory power of each independent variable on the dependent variables after preliminary PLS analysis. For example, assuming there is a dependent variable y and the independent variables are x_1, x_2, …, xk. Eq. (1) gives the VIP value of independent variable number j:

$$\mathrm{VIP_j} = \sqrt{\frac{\mathrm{k}}{\sum_{h=1}^{m} r^2(y, c_h)} \sum_{h=1}^{m} r^2(y, c_h) w_{hj}^2} \tag{1}$$

where k is the number of independent variables; c_h is the principal component extracted from the relevant independent variables; r (y, c_h) is the correlation coefficient of the dependent variable and the principal component, representing the explanatory power of the principal component to y; and w_{hj} is the weight of the independent variable on principal component. Since the explanatory power of x_j to y is conveyed through the principal component c_h, if the explanatory power of c_h to y is very strong and the effect of x_j to c_h is very significant, it can be considered that the explanatory power of x_j to y is strong.

The VIP value of each independent variable represents the explanatory power of the independent variable on the dependent variable, also known as the importance level of the independent variable for the modeling. If a reasonable VIP threshold is set for selecting high VIP-value independent variables and excluding low-valued independent variables, the accuracy of the model would not be affected much but the complexity of the model would be greatly reduced. This will a have great impact on the system speed, ease of use and cost (Wu et al., 2015).

2.2. Differential absorption dural hematoma detection

Fig. 1 shows the diagram of brain hematoma detection using multi-channel differential absorption spectrophotometry. In the diagram, S and S' are the incident light source. D_1-D_n and D'_1-D_n' are the light detectors placed at equal interval space respectively. The detection was conducted on symmetrical positions of the human head (Shareef et al., 2017). First, the detection was conducted on the right side of the head (R site) once, and the light intensities detected by n detectors were I_1-I_n respectively. Then, detection was performed on the left side of the head (L site) and the light intensities detected by the n detectors were I'_1-I_n' respectively. I_0 was the incident light intensity from both the left and the right sides. By using Eqs. (2) and (3), the light absorbance at each location OD_1-OD_n and OD'_1-OD_n'can be obtained respectively.

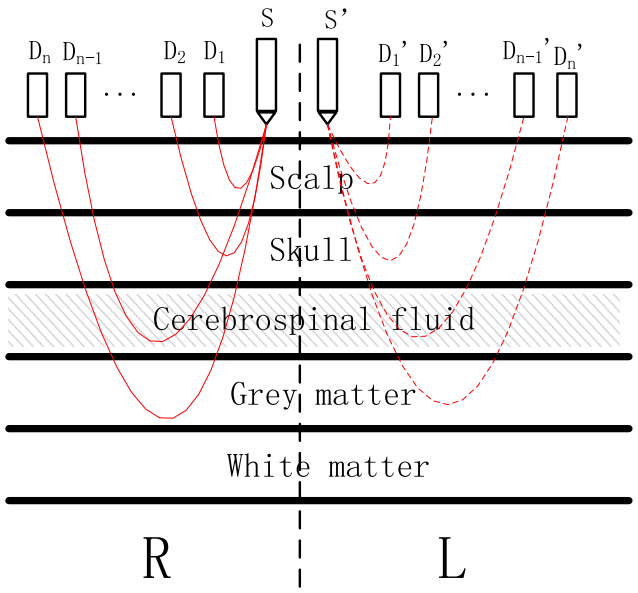

Fig. 1. The structure of brain model.

$$OD_i = \lg\left(\frac{I_0}{I_i}\right), \quad (i = 1, 2, \ldots, \mathrm{n}) \tag{2}$$

$$OD'_i = \lg\left(\frac{I_0}{I'_i}\right), \quad (i = 1, 2, \ldots, \mathrm{n}) \tag{3}$$

By dividing the light absorbance from symmetrical locations, the differential absorbance can be calculated.

$$\Delta OD_i = \frac{OD_i}{OD'_i} = \frac{\lg\frac{I_0}{I_i}}{\lg\frac{I_0}{I'_i}} = \lg\frac{I'_i}{I_i}, \quad (i = 1, 2 \ldots, 5) \tag{4}$$

According to the anatomy of the human brain, the brain model consists of 5 layers, namely, the layers of scalp, skull, cerebrospinal fluid (CSF), grey matter, and white matter (Fig. 1). The brain structure and optical parameters at 840 nm wavelength are shown in Table 1 (Holmes et al., 1996; Umeyama and Yamada, 2009). The definitions of the brain parameters are as follows: n is the refractive index; μ_a (cm^{-1}) is the absorption coefficient; μ_s (cm^{-1}) is the scattering coefficient; g is the anisotropic factor; d (cm) is the tissue thickness.

Monte Carlo simulation was used to establish the brain model in this study. Monte Carlo simulation can describe the transmission path of photons within any tissue structure. It is considered as the simulation most close to reality and is known as the "golden standard" in describing photon transmission trajectory in biological tissue (Jamal et al., 2017). The simulated photon number in this study was set as 10^8. According to the study by Strangman et al., the thickness of the human scalp is 6.9 ± 3.6 mm and the thickness

Table 1
Brain model optical parameters.

Brain Layer	n	μ_a (cm^{-1})	μ_s' (cm^{-1})	g	d (cm)
Scalp	1.45	0.21	18.1	0.9	d1
Skull	1.45	0.19	15.2	0.9	d2
CSF	1.45	0.05	2.3	0.9	0.2
Grey matter	1.45	0.42	20.9	0.9	0.4
White matter	1.45	0.17	86.5	0.9	3.4

of the skull is 6.0 ± 1.9 mm. In this study, the thickness of the scalp and skull were set as 1.3 cm, of which the thickness of the scalp was 7.0 mm and the thickness of skull was 6.0 mm (Strangman et al., 2014).

Clinical cerebral hematoma can be categorized as subdural hematoma, epidural hematoma, intracerebral hematoma and subarachnoid hemorrhage. Most hematomas caused by traumatic brain injury are positioned extradurally or intradurally under the skull, which is located at the third level, i.e. the cerebrospinal fluid level in the brain model (Bullock et al., 2006; Abbas et al., 2017). When traumatic brain hematoma occurs, the absorption coefficient of the dural position will increase significantly. Clinical studies have shown that the hematoma absorption coefficient increases over 10 times, while the normal dural position absorption coefficient is 0.05 cm^{-1}. In order to simulate different degrees of hematoma, in this study, the dural position μ_a was set at a range of 0.5–1.5 cm^{-1} and the adjustment step length was 0.1 cm^{-1}.

2.3. Data processing and VIP screening of detector position

2.3.1. Data processing

According to Monte Carlo simulation, the luminous fluxes from 30 detectors placed at different radial positions from the light source were obtained. The ΔOD values of the detectors located within a 2.0–5.0 cm range with a 0.1 cm interval were calculated using Eq. (4). White noise is the random noise evenly distributed throughout the frequency spectrum with similar energy density and it exists in every detector. In this study, white noise was added to the ΔOD value in each detector according to the signal-to-noise ratio of the spectrometer in order to verify the robustness of the model. The USB2000+ fiber optic spectrometer from Ocean Optics is the most classic and popular spectrometer. It is suitable for many types of scientific studies and industrial applications. Its signal-to-noise ratio is 250:1. This ratio was used as a basis for the added white noise in this study. The PLS model was built using ΔOD values with added white noise from the detectors at each position as the input and the dural position μ_a as the output.

2.3.2. VIP screening of detector position

The VIP values of the difference in luminous flux ΔOD of detectors at different position versus the hematoma degree y were calculated based on the definition of the importance of variable projection of Eq. (1). The result is shown in Fig. 2.

The importance of each detector position on modeling can be viewed clearly using the VIP radial distribution map between 2.0 cm and 5.0 cm. Based on the characteristics of the brain structure as well as the VIP values, the chosen screening criterion for the detector position was that the normalized VIP value should be greater than 0.14. As shown in the radial distribution map of VIP in Fig. 4, the detector positions at 2.1 cm, 2.4 cm, 3.4 cm and 4.2 cm met the screening criteria. After VIP screening, the ΔOD values with the added white noise from the 4 detector positions were used as the input and the dural position μ_a as the output to establish the PLS model. The model verification method used was Leave-

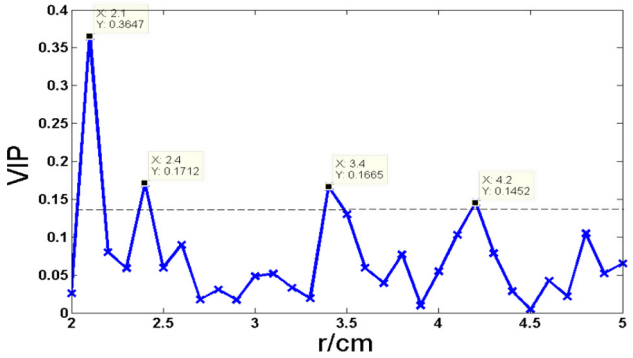

Fig. 2. Radial distribution map of VIP.

One-Out Cross Validation (LOOCV) and the model extraction fraction was 2.

3. Results and discussions

One experimental group and two control groups were used for this study. The experimental group was modeled using the VIP screening result. Control group 1 underwent PLS modeling using the ΔOD values from 30 detectors positioned at 2.0–5.0 cm with a 0.1 cm division as the input. Control group 2 underwent PLS modeling using the ΔOD values from 4 detectors located at 2.0 cm, 3.0 cm, 4.0 cm and 5.0 cm from the light source as the input and the dural position μ_a as the output. White noise was added to all models. The prediction results are shown in Fig. 3. Fig. 3(a) shows the results of the dural position μ_a prediction PLS model using the 4 selected VIP detectors. The model correlation was 99.48%; the mean error was 0.0200 cm^{-1}; and the maximum error was 0.0414 cm^{-1}. Fig. 3(b) shows the results of the dural position μ_a prediction PLS model of control group 1 using 30 detectors. The model correlation was 98.54%; the mean error was 0.0339 cm^{-1}; and the maximum error was 0.0684 cm^{-1}. Fig. 3(c) shows the results of the dural position μ_a prediction PLS model of control group 2 using 4 equally positioned detectors. The model correlation was 97.26%; the mean error was 0.0474 cm^{-1}; and the maximum error was 0.0814 cm^{-1}.

The comparison of the relative errors (RE) among the three different model groups is shown in Fig. 4. The experiment group modeled via the PLS model used the ΔOD from 4 detectors with distances of 2.1 cm, 2.4 cm, 3.4 cm and 4.2 cm from the light source respectively to predict the dural position μ_a. The RE was 2.06%. The control group 1 PLS model used the ΔOD from 30 detectors to predict the dural position μ_a. The RE was 4.08%. Control group 2 PLS model used the ΔOD from 4 equally distanced detectors 2.0 cm, 3.0 cm, 4.0 cm and 5.0 cm from the light source to predict the dural position μ_a. The RE was 5.68%. These results show that the model with the 4 detectors selected through the VIP method has the smallest RE. Therefore, satisfactory results of dural position μ_a prediction using VIP for the selection of detector position and number can be obtained.

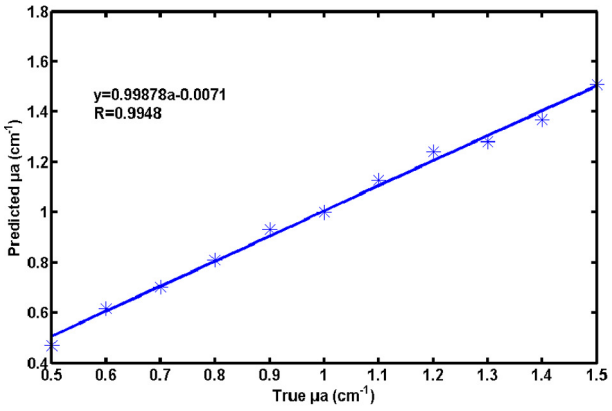

(a)

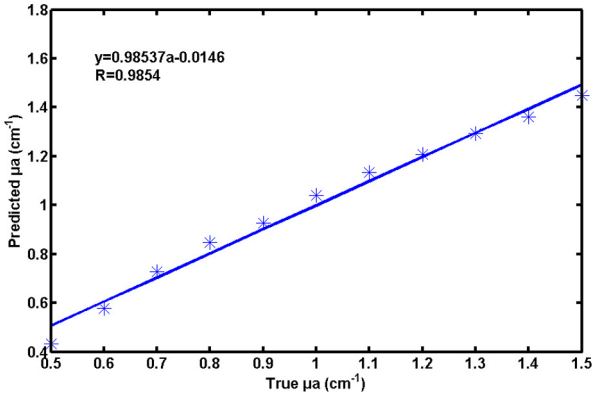

(b)

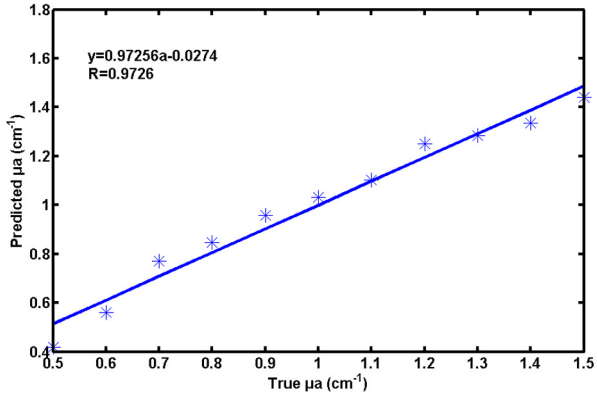

(c)

Fig. 3. μ_a predicated result with PLS. (a) μ_a predicated result with PLS model of experiment group. (b) μ_a predicated result with PLS model of control group 1. (c) μ_a predicated result with PLS model of control group 2.

4. Conclusion

In this study, variable importance in the projection (VIP) method was used to simplify the model that uses differential near-infrared luminous flux for the detection of the position μ_a. A highly accurate model with smaller relative error can be built using a smaller number of detectors using VIP screening for detectors with different radial distances from the light source. This study is important for the miniaturization and portability of brain hematoma detection device research. It plays an important role in the promotion of portable near-infrared brain hematoma detector applications in complex environments and provides an important reference and a new direction for the research on relationship between the location of detectors and source and the effective depth of photons.

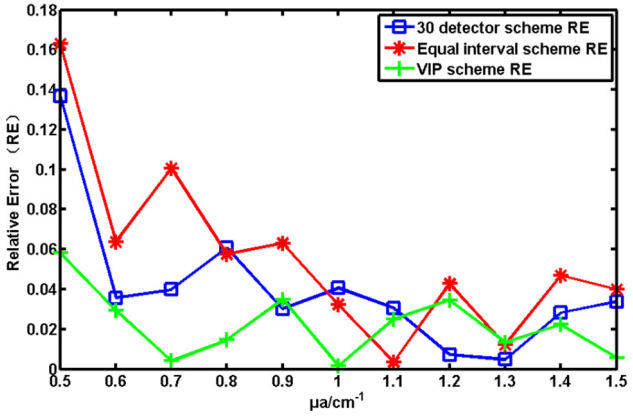

Fig. 4. Map of RE.

Acknowledgments

The work described in this paper was fully supported by a grant from the Tianjin Science and Technology Project of China (No. 13ZCZDSY20100) and the National Science Foundation of Tianjin (No. 15JCQNJC14500), besides, the paper was supported by the Key Laboratory of Biomedical Effects of Nanomaterials and Nanosafety, CAS (No: NSKF201602).

References

Abbas, G., Salman, A., Rahman, S.U., Ateeq, M.K., Usman, M., Sajid, S., Zaheer, Z., Younas, T., 2017. Aging mechanisms: linking oxidative stress, obesity and inflammation. Matrix Sci. Med. 1 (1), 30–33.
Bergdahl, M., Bergdahl, J., 2000. Low unstimulated salivary flow and subjective oral dryness: association with medication, anxiety, depression, and stress. J. Dent. Res. 79 (9), 1652–1658.
Braun, T., Kunz, U., Schulz, C., et al., 2015. Near-infrared spectroscopy for the detection of traumatic intracranial hemorrhage: feasibility study in a German army field hospital in Afghanistan. Der Unfallchirurg 118 (8).
Broderick, G., Craddock, R.C., Whistler, T., et al., 2006. Identifying illness parameters in fatiguing syndromes using classical projection methods. Pharmacogenomics 7 (7), 407–419.
Bullock, M.R., Chesnut, R., Ghajar, J., et al., 2006. Surgical management of posterior fossa mass lesions. Neurosurgery 58 (3 Suppl), S47–S55. discussion Si-iv.
Gao, W. et al., 2017. The first multiplication atom-bond connectivity index of molecular structures in drugs. Saudi Pharm. J. 25 (4), 548–555.
Halim, N.I.A., Phang, I.C., 2017. Salicylic acid mitigates pb stress in nicotiana tabacum. Galeri Warisan Sains 1 (1), 16–19.
He, W.Q., Yan, W.J., He, G.Q., et al., 2016. Study on the wavelength selection based on VIP analysis in noninvasive measurement of blood components. Spectrosc. Spectral Anal. 36 (4), 1080.
Hitoshi, Y., Takasei, M., Tomonori, Y., et al., 2016. Head computed tomographic measurement as a predictor of outcome in patients with subdural hematoma with cerebral edema. Scand. J. Trauma Resuscit. Emerg. Med. 24 (1), 1–6.
Holmes, C.J., Hoge, R., Collins, L., et al., 1996. Enhancement of MR images using registration for signal averaging. J. Comput. Assist. Tomogr. 22 (2), 324–333.
Jamal, M., Shareef, M., Sajid, S., 2017. Lincomycin and tetracycline resistance in poultry. Review. Matrix Sci. Pharm. 1 (1), 33–38.
Kato, S., Yoshitani, K., Ohnishi, Y., 2015. Cerebral Blood flow measurement by near-infrared spectroscopy during carotid endarterectomy. J. Neurosurg. Anesthesiol.
Kim, B., Kim, K., Im, K.H., et al., 2016. Multiparametric MR imaging of tumor response to intraarterial chemotherapy in orthotopic xenograft models of human metastatic brain tumor. J. Neuro-Oncol. 127 (2), 243–251.
Nourhashemi, M., Mahmoudzadeh, M., Wallois, F., 2016. Thermal impact of near-infrared laser in advanced noninvasive optical brain imaging. Neurophotonics 3 (1).
Robertson, C.S., Gopinath, S., Chance, B., 1997. Use of near infrared spectroscopy to identify traumatic intracranial, hemotomas. J. Biomed. Opt. 2 (1), 31–41.
Shamsudin, N.H., Wong, C.F., Rahman, R.N.Z.R.A., Ali, M.S.M., 2017. Tight repression of elastase strain K overexpression by Pt7 (A1/O4/O3) shuttle expression system. GaleriWarisanSains 1 (1), 20–22.

Shareef, M., Jamal, M., Sarfraz, M., 2017. A review of Anti-bacterial activity of Nigella sativa in gut of broiler chicks. Matrix Sci. Pharma 1 (1), 27–32.
Shi, Z., Song, J.X., et al., 2017. Effects of preoperative psychological intervention on early postoperative cognitive dysfunction after off-pump coronary artery bypass surgery. Biomed. Res. 28 (7), 2909–2912.
Strangman, G.E., Quan, Z., Zhi, L., 2014. Scalp and skull influence on near infrared photon propagation in the Colin27 brain template. Neuroimage 85 (2), 136–149.
Umeyama, S., Yamada, T., 2009. Monte Carlo study of global interference cancellation by multidistance measurement of near-infrared spectroscopy. J. Biomed. Opt. 14 (6), 717–722.
Wang, X.N., Wei-Tao, L.I., Qian, Z.Y., et al., 2011. Near infrared effective detection depth in mouse traumatic brain edema model. Acta Photon. Sin. 40 (2), 277–281.
Wu, X., Eggebrecht, A.T., Ferradal, S.L., et al., 2015. Evaluation of rigid registration methods for whole head imaging in diffuse optical tomography. Polis 2 (3), 1–7.
Yildirim, N., Simsek, M., et al., 2017. Early onset of radiation induced sarcoma: a case report and review of the literature. Acta Med. Mediterr. 33 (4), 565–568.
Zeng, T., Cun-Yong, J.U., Cai, T.J., et al., 2010. Selection of parameters for estimating canopy closure density using variable importance of projection criterion. Beijing Linye Daxue Xuebao/J. Beijing Forest. Univ. 32 (6), 37–41.